PARTON DISTRIBUTIONS*

A.D. MARTIN

Department of Physics, University of Durham
Durham DH1 3LE, England

(Received October 1, 1991)

We briefly review the parton model and give reasons why an accurate determination of the parton distributions is important. We summarize the recent determinations of the parton distributions of the proton and describe the role played by deep inelastic lepton-nucleon scattering and related data. We compare the determination of $\alpha_s(M_Z)$ from deep inelastic scattering with the average of the LEP measurements. We use a simple model to illustrate why the Lipatov equation predicts a small x behaviour of the gluon distribution of the form $xg \sim x^{-\lambda}$ with $\lambda \simeq 0.5$. We describe how shadowing contributions suppress this singular behaviour and we discuss a structure function analysis which incorporates these effects at small x. We introduce the GLR equation and outline how an explicit numerical solution has been obtained for the behaviour of the gluon distribution at small x. We mention various future experimental probes of the small x region.

PACS numbers: 12.40.-y

1. Partons

The classic way to investigate the structure of the proton is to scatter electrons off it; indeed the technique has just claimed its second Nobel Prize [1]. According to quantum mechanics an electron beam of momentum p has a possible spatial resolution $\lambda \sim 1/p$, and so the higher the energy of the beam the more detailed is the structure probed. We use units with $\hbar = 1$ (and $c = 1$).

First consider the scattering of a beam of electrons of energy E from a stationary nuclear target of mass M_N. The kinematic variables are shown in

---

* Presented at the XXXI Cracow School of Theoretical Physics, Zakopane, Poland,June 4-14, 1991.

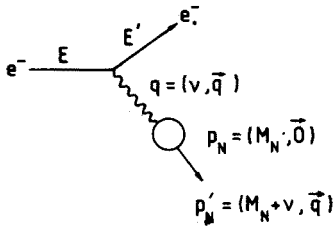

Fig. 1. Kinematic variables for electron-nucleus scattering in the laboratory frame.

Fig. 1, where, in particular, the outgoing 4-momentum is $p'_N = (M_N + \nu, \vec{q})$. Thus for elastic scattering we have

$$p'^2_N = M^2_N = (M_N + \nu)^2 - \vec{q}^2$$

and so the electron energy loss, $\nu = E - E'$, is given by

$$\nu = \frac{Q^2}{2M_N},$$

where $-Q^2 \equiv q^2 = \nu^2 - \vec{q}^2$ is the 4-momentum transfer squared carried by the photon probe. The larger the value of Q^2 the more deeply we probe the structure of the nucleus, as shown by the succession of sketches shown in Fig. 2. We notice the reduction of the electron-nucleus elastic scattering peak with increasing Q^2, indicating that the nucleus possesses a structure; the harder the nucleus is probed the less likely it is to remain intact. (If the nucleus were structureless we would simply see the elastic peak at $x_N \equiv Q^2/2M_N\nu = 1$). At high Q^2, namely $Q^2 \gg 1/R^2$, we see that the scattering takes place from individual nucleons within the nucleus, and that the electron-nucleon elastic scattering peak occurs at $\nu = Q^2/2M$ (where M is the nucleon mass), but with the peak smeared out due to the Fermi momentum of the nucleons confined in the nucleus.

High energy electron-proton scattering can be regarded as a replay of electron-nucleus scattering, where now the constituents are the (three valence) quarks confined within the proton (see Fig. 3). The continuous curve shows the electron-quark elastic scattering peak, plotted in terms of the Bjorken scaling variable

$$x = \frac{Q^2}{2M\nu}, \tag{1}$$

where now the peak is smeared out by the Fermi momentum of the quarks bound in the proton. However the proton is not simply composed of three point-like quarks, and at higher Q^2 we see violations of the "scaling" curve arising, for example, from the photon probing one of a pair of "sea" quarks

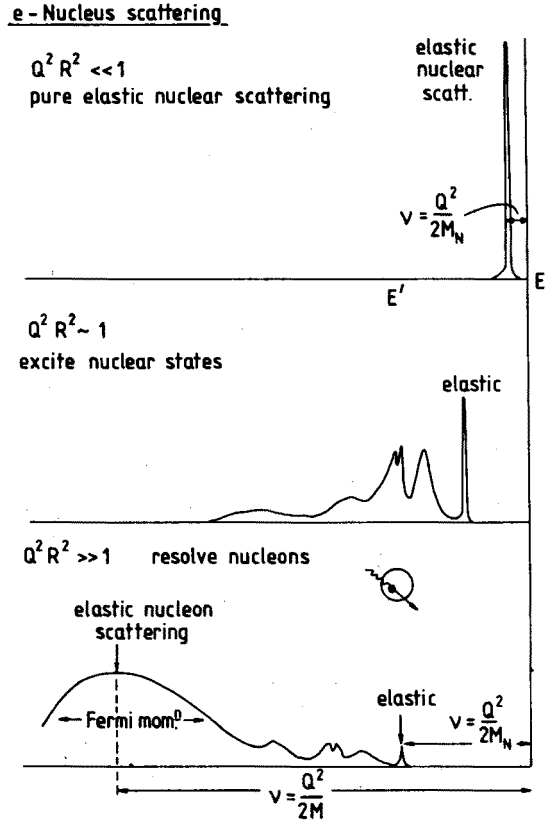

Fig. 2. Schematic illustration of the cross section for electron-nucleus scattering as a function of E' at three different values of Q^2. The distance, $\nu = E - E'$, from the right-hand axis is the energy loss in the laboratory frame. R is the radius of the nucleus.

which originate from a gluon ($g \rightarrow q_{sea}\bar{q}_{sea}$) itself radiated from one of the valence quarks, see the sketch at the bottom of Fig. 3. That is, the resolution increases with increasing Q^2 so that the apparent number of partons which share the proton's momentum increases, and hence there is an increased chance of finding a quark at small x and a decreased chance of finding one at high x. Thus these QCD effects modify the scaling curve to the dashed curve, which gradually "skews" more and more towards small x as Q^2 increases.

The constituents or "partons" of the proton are the valence and sea quarks and the gluons. In the naive parton model we ignore the fact that a quark may radiate gluons, before and/or after being probed by the photon, but for detailed studies we must include these QCD effects.

The distribution of partons within the proton is primarily determined

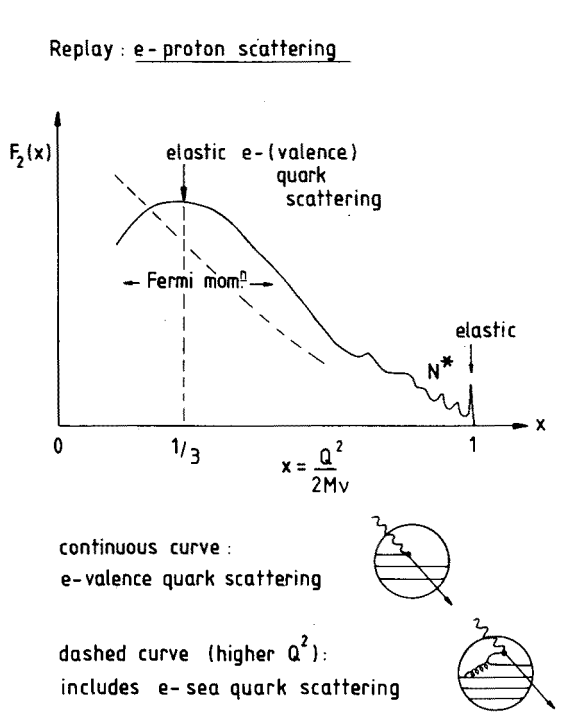

Fig. 3. Schematic illustration of electron-proton scattering as a function of the scaling variable x. The scaling violations, arising from QCD effects, lead to the dashed curve which skews more towards small x as Q^2 increases.

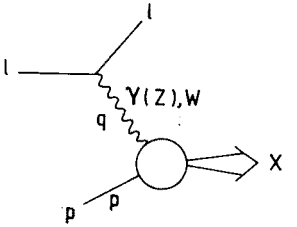

Fig. 4. Deep inelastic lepton-proton scattering, $\ell\, p \to \ell X$. The processes $ep \to eX$ and $\nu\, p \to \mu X$, for example, proceed *via* γ (or Z) and W exchange respectively.

by deep inelastic lepton-nucleon scattering. The generic process is sketched in Fig. 4. The lower or hadronic vertex is described by two kinematic variables: $Q^2 = -q^2$ and the Bjorken scaling variable $x = Q^2/2p \cdot q$. The general expression for the photon exchange contribution to $ep \to eX$, for example, is, for $E \gg M$,

$$\frac{\partial^2 \sigma^\gamma}{\partial x \partial Q^2} = \frac{8\pi\alpha^2 ME}{Q^4}\left(\frac{1+(1-y)^2}{2} 2xF_1 + (1-y)(F_2 - 2xF_1)\right), \quad (2)$$

where $y = \nu/E$ in the laboratory frame, and so deep inelastic scattering experiments determine the structure functions $F_i(x, Q^2)$.

In the naive parton model the lower vertex of Fig. 4 can be expressed in terms of scattering from individual quarks, as shown in Fig. 5, and we find

$$F_2(x, Q^2) = \sum_q e_q^2 x f_q(x), \tag{3}$$

$$F_1(x, Q^2) = \frac{1}{2x} F_2(x, Q^2), \tag{4}$$

where $f_i(x)$ is the probability that the struck parton i carries a fraction x of the momentum of the proton. Equality (4), which is only true in the naive model, is a direct consequence of the spin $^1/_2$ character of the quarks. Also we see that in this model the structure functions are predicted to be functions of a single variable x, which can be identified with that given in (1) since from Fig. 5 we have

$$(xp + q)^2 = m_q^2. \tag{5}$$

If we go to a frame in which the proton is moving with infinite momentum we may neglect masses and so (5) gives

$$x = \frac{-q^2}{2p.q} \left[= \frac{Q^2}{2M\nu} \right]_{\text{lab.}}.$$

In the infinite momentum frame, relativistic time dilation slows down the rate at which the partons interact with one another, and so the photon probes an essentially free particle. We implicitly used this incoherence assumption in writing the summation in Fig. 5, which represents an addition of probabilities (not amplitudes) of scattering from single free partons.

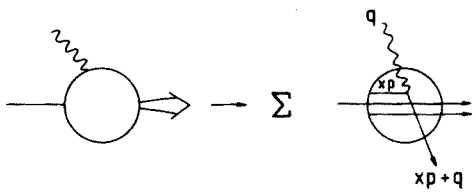

Fig. 5. The naive parton model approximation of the hadronic vertex of Fig. 4. The sum is over all the quarks in the proton; p is the 4-momentum of the proton.

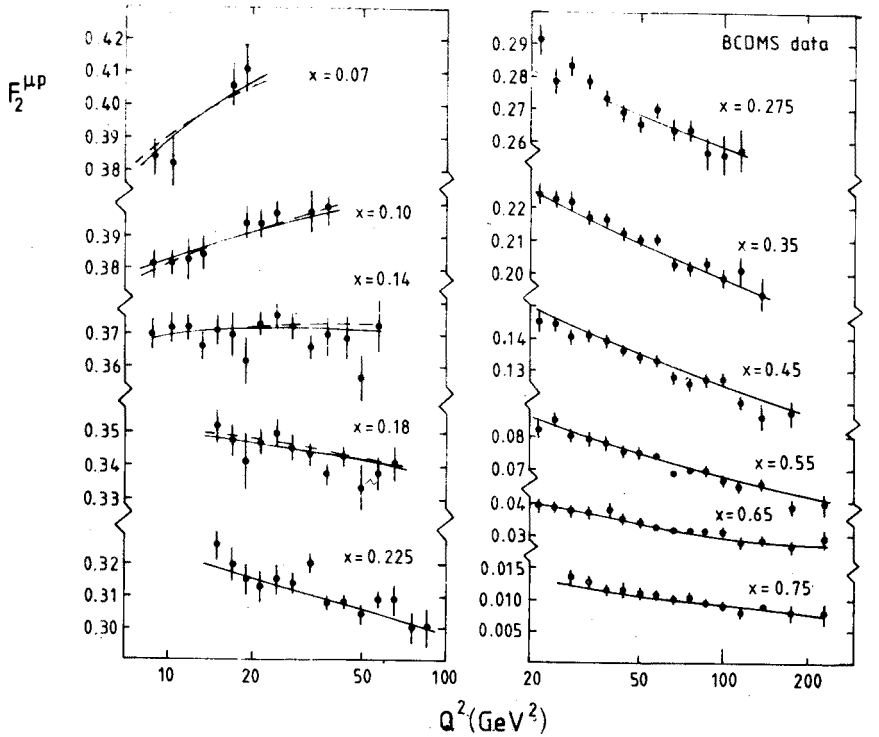

Fig. 6. The measurements of the structure function $F_2(x, Q^2)$ of deep inelastic $\mu p \to \mu X$ scattering obtained by the BCDMS collaboration [2]. The curves show the fit by the KMRS [3] partons.

In the QCD-improved parton model we expect that there will be violations of the scaling properties of the structure functions, with F_i increasing (decreasing) logarithmically as Q^2 increases at small (large) values of x, as implied by Fig. 3. These QCD scaling violations are clearly visible in the data, as can be seen, for example, from Fig. 6. Similarly the parton distributions themselves, $f_i(x, Q^2)$ are functions of Q^2, as well as of x.

2. Why parton distributions are important

Twenty or so years after the pioneering experiments on deep inelastic scattering and their description in terms of partons, it is relevant to ask why we should continue to devote so much time to the study of the distributions of partons within hadrons, and within the proton in particular. So first, we present some of the reasons why they continue to attract so much attention [4].

A knowledge of parton distributions is an essential ingredient in all "hard" hadron interactions. As the introductory discussion implies, they are determined primarily from deep inelastic lepton-nucleon scattering data. In the QCD parton model the cross section has the factorizable form

$$\sigma^{\ell N} = \sum_{i=q,\bar{q},g} f_i^N \otimes \hat{\sigma}^{\ell i}, \tag{6}$$

where the parton distribution, $f_i^N(x, Q^2)$, represents the probability that parton i of the nucleon N is found to carry fraction x of its momentum when probed with 4 momentum-transfer-squared $q^2 \equiv -Q^2$. Here we use $\otimes$ to imply integration over the allowed range of x. The partonic or subprocess cross sections $\hat{\sigma}$ can be calculated using QCD perturbation theory. The next-to-leading order QCD contributions are known and this, together with the considerable improvement in the precision of the deep inelastic μN and νN scattering data, has enabled the parton distributions to be determined with a reasonable degree of confidence, at least in the range $0.03 \lesssim x \lesssim 0.8$. The parton distributions are universal provided, of course, they are defined consistently. That is, when due account is taken of the renormalization scheme, they can be used to predict the cross section for any hard hadronic process, for example the production of a state A at the high energy $p\bar{p}$ colliders

$$\sigma^{p\bar{p}\to AX} = \sum_{i,j} f_i^p \otimes f_j^{\bar{p}} \otimes \hat{\sigma}^{ij\to A}. \tag{7}$$

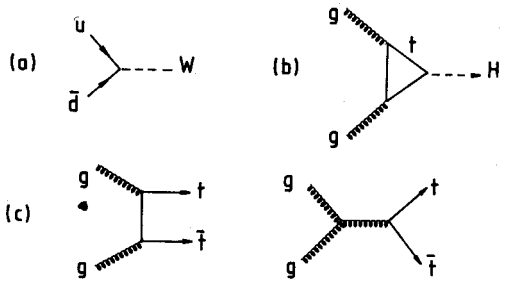

Fig. 7. Lowest order contributions to W, H and t hadroproduction.

We show the leading order QCD subprocess for three topical processes in Fig. 7, namely for W and Higgs boson, and top quark production. For each process accurate knowledge of the parton distributions is important. In the first example the error associated with the measurement of the W boson mass, M_W, at the $p\bar{p}$ colliders has a sizeable contribution arising from the uncertainties in the parton distributions. (Now that M_Z is so accurately determined, M_W is a key and limiting parameter in the electroweak tests of the standard model). Fig. 7(b) shows that an estimate of the cross section for the production of a Higgs boson of mass $M_H = 100$ GeV, say, at the

SSC ($\sqrt{s}$ = 40 TeV) would require knowledge of the gluon distribution in a proton at x values in the region $x \sim M_H/\sqrt{s} \sim$ few $\times 10^{-3}$. The final example, Fig. 7(c), shows that if the mass of the top quark, m_t, is to be measured from the rate of $t\bar{t}$ production then again the accuracy will depend on the precision with which the parton distributions are known.

Indeed the universal character of the parton distributions, together with a knowledge of the higher order QCD contributions, allows a wide range of processes to be inter-related with considerable precision. In fact the high statistics data which now exist for many of these processes enable detailed QCD consistency tests to be performed. An example is shown in Fig. 8, which compares the jet cross section measured by the CDF collaboration with a zero-parameter QCD prediction [5].

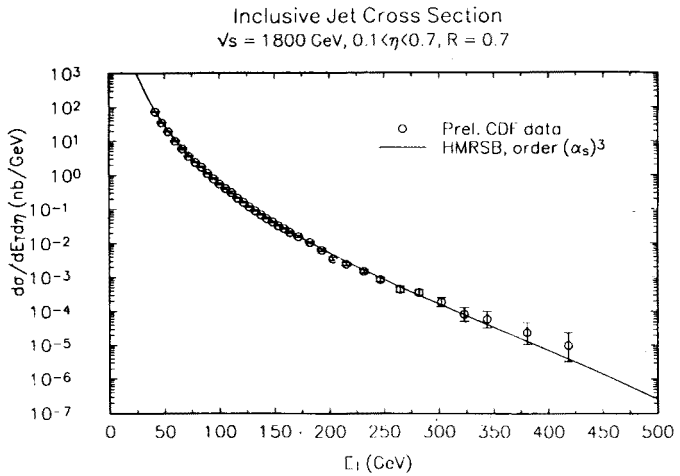

Fig. 8. Measurements of the jet cross section $d\sigma/d\eta dE_T$ at $\sqrt{s} = 1.8$ TeV by the CDF collaboration, compared with an $O(\alpha_s^3)$ QCD prediction [5] averaged over the CDF fiducial region $0.1 < |\eta| < 0.7$.

A related reason for the current interest in parton distributions is that the next-to-leading order QCD analyses of deep inelastic data allow a precision measurement of Λ_{QCD}, and hence of $\alpha_s(M_Z)$, which is competitive with the recent independent determination of the strong coupling from the LEP experiments.

The final reason why parton distributions are of topical interest concerns their behaviour at very small values of x, by which we mean $x \sim 10^{-3}$. As we have seen, knowledge of this behaviour is needed to estimate the rates of the various hard processes at LHC and SSC energies. However the partonic behaviour at small x is particularly interesting in its own right, as new theoretical effects occur. Indeed it is said [6] that, apart from confinement,

small x is the most interesting problem in QCD.

3. Present knowledge of parton distributions

The distributions of the quarks and gluons within the proton are primarily determined by analyses of the structure functions $F_i(x, Q^2)$ measured in muon (or electron)-nucleon (or nucleus) and neutrino-nucleus deep inelastic scattering. Each of the structure functions can be expressed as a linear sum of the parton distributions

$$F_i(x, Q^2) = \sum_j c_{ij} f_j(x, Q^2) \tag{8}$$

and the basic procedure is to parametrize the f_i at a sufficiently large Q_0^2, say 4 or 5 GeV^2, so that $f_i(x, Q^2)$ can be calculated perturbatively at higher Q^2 using either evolution equations typically of the form

$$\frac{\partial g(x, Q^2)}{\partial \log Q^2} = \frac{\alpha_s}{2\pi} \int_x^1 \frac{dy}{y} \left(P_{gg}\left(\frac{x}{y}\right) g(y, Q^2) + \sum_i P_{gq}\left(\frac{x}{y}\right) q_i(y, Q^2) \right) \tag{9}$$

or a Mellin transform analysis. The parton splitting functions in (9), which specify the probabilities that the processes shown in Fig. 9 occur, are given by

$$P_{gg}(z) = 6\left(\frac{z}{1-z} + \frac{1-z}{z} + z(1-z)\right), \quad P_{gq}(z) = \frac{4}{3}\frac{1+(1-z)^2}{z}, \tag{10}$$

where we have omitted the virtual gluon corrections which tame the $z = 1$ singularity of P_{gg}. Similar expressions determine the Q^2 evolution of the $q_i(x, Q^2)$. It is usually assumed that Q_0^2 is sufficiently large for higher twist contributions to be ignored.

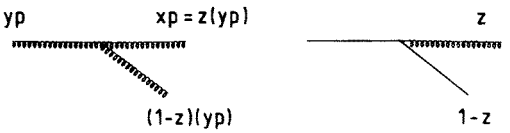

Fig. 9. Parton splitting processes with momentum fractions relevant for Eq. (9), with $z = x/y$. Note from (10) that the probability of emitting a soft gluon is given by $P_{gg}(z) \sim 6/z$ and $P_{gq} \sim (8/3)/z$ respectively.

A typical parametrization at $Q^2 = Q_0^2$ of the valence, sea and gluon distributions of the proton is of the form

$$xu_v = N_1 x^{\eta_1}(1-x)^{\eta_2}(1+\eta_3 x), \tag{11}$$

$$xd_v = N_2 x^{\eta_4}(1-x)^{\eta_5}(1+\eta_6 x), \tag{12}$$

$$2x(\bar{u}+\bar{d}+\bar{s}) = A_s x^{-\lambda}(1-x)^{\eta_s}, \tag{13}$$

$$xg = A_g x^{-\lambda}(1-x)^{\eta_g}, \tag{14}$$

where $u_v = f_u^p - f_{\bar{u}}^p$ etc. There are thus ten or so free parameters (eight η_i, A_s (or A_g) and Λ_{QCD}) to be determined by fitting to a wide range of deep inelastic scattering and related data for $Q^2 > Q_0^2$. The coefficients N_1, N_2 are fixed by the flavour sum rules, and A_g (or A_s) by the momentum sum rule. Generally it is assumed that the sea quarks satisfy $\bar{u} = \bar{d} = 2\bar{s}$, where the relative weakness of the strange sea is indicated by ν induced dimuon production data [7], although the flavour content of the sea remains an open question and, prompted by recent NMC data [8], has recently been the subject of much theoretical speculation. The contribution of the charm and bottom sea is also usually included *via* $g \to Q\bar{Q}$. Naive quark parton model and Regge arguments (with unit Pomeron intercept) imply that $\lambda = 0$ in (13) and (14). However, as we shall discuss below, there are theoretical reasons why λ may be as large as 0.5 and some of the recent analyses have presented sets of partons obtained using this value.

Such determinations of the parton distributions from deep inelastic data have a long history starting from the original work by Feynman–Field and Buras–Gaemers, and followed by the parametrizations of Glück–Hoffmann–Reya [9], Duke–Owens [10] and Eichten–Hinchliffe–Lane–Quigg [11] which subsequently have been widely used. These are all leading order QCD analyses of the deep inelastic data that were available up to about 1983. Over the last three or so years there has been considerable improvement in the precision of both muon [2,8,12] and neutrino [13,14] deep inelastic data, which has stimulated more detailed structure function analyses [3,15-21] which include the next-to-leading order (NLO) QCD contributions. To better determine the parton distributions these analyses supplement the deep inelastic data with recent high precision data for prompt photon production and/or the production of Drell–Yan pairs.

We sketch below the constraints imposed by the various data. The deep inelastic data pin down the quark distributions (*cf.* Eq. (3)),

$$\frac{1}{x}F_2^{\mu p} = \frac{4}{9}u + \frac{1}{9}d + \ldots, \tag{15}$$

$$\frac{1}{x}F_2^{\mu n} = \frac{1}{9}u + \frac{4}{9}d + \ldots, \tag{16}$$

$$\frac{1}{x}F_2^{\nu N} = \Sigma(q + \bar{q}) + \ldots, \tag{17}$$

$$F_3^{\nu N} = \Sigma(q - \bar{q}) + \ldots, \tag{18}$$

but hardly constrain the gluon distribution, which only enters directly at NLO; essentially the only constraint is the momentum sum rule which shows that the gluon carries just less than 50% of the proton's momentum at Q_0^2. On the other hand the gluon enters at leading order in prompt photon production. Indeed for "large" p_T photons produced by $pp \to \gamma X$, the dominant QCD subprocess is $gq \to \gamma q$, in contrast to $p\bar{p} \to \gamma X$ where the annihilation process $q\bar{q} \to \gamma g$ is much more important. The most relevant $pp \to \gamma X$ data are due to the WA70 collaboration [22] with p_T in the range 4 to 6 GeV/c, which measure the gluon in the region of $x \sim 0.4$. Combined with the momentum sum rule constraint this is sufficient to determine that $\eta_g \sim 5$, the value of the gluon exponent anticipated by the naive spectator quark counting rules. Finally data for the Drell–Yan process, $pN \to \mu^+\mu^- X$, which is mediated by $q_v\bar{q}_s \to \gamma^*$, primarily constrain the exponent η_s of the sea quark distributions.

TABLE I

NLO determinations of parton distributions, and the deep inelastic scattering and related data [2,8,12-14,22-24] that were used in the various global analyses. In addition deep inelastic CCFRR ν data [14] and SLAC e data [25] have been used. The discrepancy between the EMC and BCDMS muon data has been largely resolved, at least for $x < 0.3$, by renormalizing the former up by 8% and the latter down by 2%, see, for example, Ref. [26].

	μ-DIS	ν-DIS	Prompt γ	D-Y	$\lambda \neq 0$	Scheme
MRS [15]	EMC + ..	CDHSW	AFS(+J/ψ)	-	Yes	$\overline{\text{MS}}$
DFLM [16]	(EMC + ..)	CHARM + ..	-	(E288 + ..)	No	DIS
ABFOW [17]	BCDMS	-	WA70	-	No	$\overline{\text{MS}}$
HMRS [18]	EMC, BCDMS, NMC	CDHSW	WA70	E605	No	$\overline{\text{MS}}$
MT [19]	EMC, BCDMS	CDHSW	-	E288,E605	Yes	DIS,$\overline{\text{MS}}$
KMRS [3]	BCDMS, NMC	CDHSW	WA70	E605	Yes	$\overline{\text{MS}}$

The recent NLO analyses are listed in Table I, together with the data fitted. We also list in this table the renormalisation scheme used in the various analyses, and whether or not non-zero values of λ of Eq. (14) have been considered. This latter point is clearly important when we come to consider extrapolations into the region of very small x.

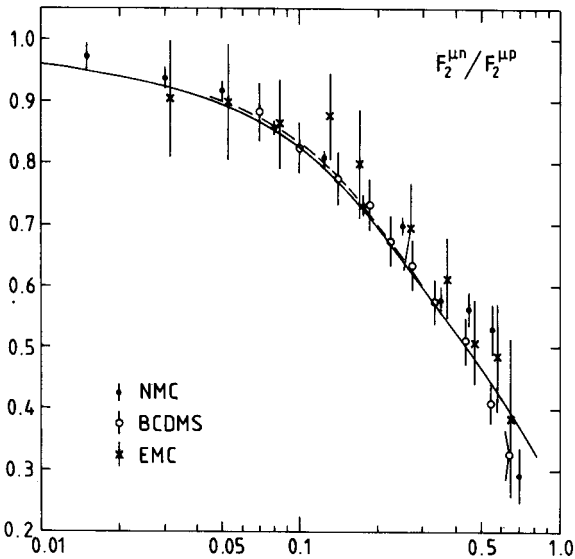

Fig. 10. The measurements of $F_2^{\mu n}/F_2^{\mu p}$ by NMC [8], BCDMS [2] and EMC [12] as fitted by KMRS [3] partons.

Typical fits, which also indicate the quality of the data, are shown in Figs 6 and 10. The n/p data of Fig. 10 are particularly important for separating the u and d quark distributions, and for making reliable predictions for W production at hadron colliders. These data play an influential role in reducing the error on the determination of M_W which arises from uncertainties in the parton distributions [27]. With the exception of the first NMC data point shown on Fig. 10 all the experimental measurements, with $Q^2 > 5$ GeV^2, relevant to the determination of partons, lie in the region

$$0.03 \lesssim x \lesssim 0.8. \tag{19}$$

However the precision of these data, together with the theoretical knowledge of the NLO contributions, mean that we now have well-constrained sets of parton distributions in this kinematic region.

4. Determination of α_s from deep inelastic data

A recent study by Amaldi *et al.* [28] of the possible unification of the standard model couplings at some large GUT scale, $M_{\rm GUT}$, has attracted a lot of interest. Using the LEP measurements of M_Z and $\sin^2\theta_W$, together with the DELPHI determination of α_s,

$$\alpha_s(M_Z) = 0.108 \pm 0.005, \tag{20}$$

Amaldi *et al.* find that the couplings are more than seven standard deviations away from meeting at a point, see Fig. 11(a). However if (minimal) supersymmetric particles (of degenerate mass $M_{\rm SUSY} = 10^3$ GeV) are added they claim the evolution of the couplings is modified in such a way that unification is achieved at $M_{\rm GUT} \sim 10^{16}$ GeV, see Fig. 11(b). The crucial parameter is α_s. If instead of (20), we use the average of the LEP determinations [29],

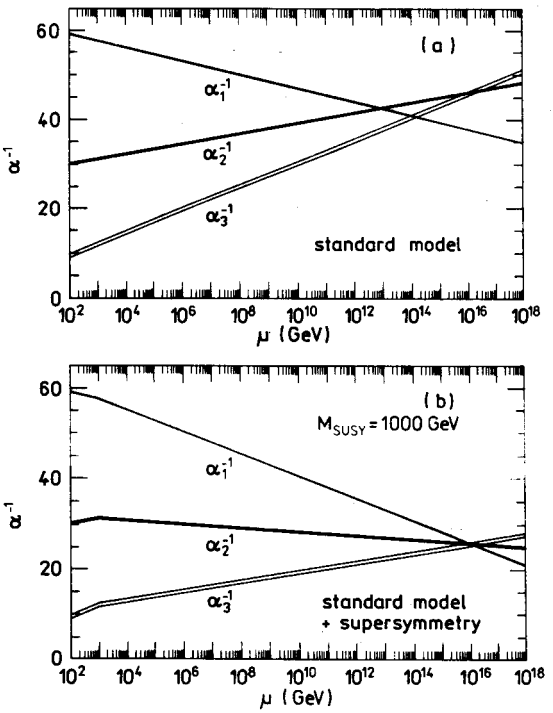

Fig. 11. The evolution of the standard model couplings (a) without SUSY, and (b) including minimal SUSY with the supersymmetric particles all of mass $M_{\rm SUSY} = 10^3$ GeV.

$$\alpha_s(M_Z) = 0.120 \pm 0.007, \tag{21}$$

then, in this simple model, it turns out that $M_{\rm SUSY}$ is predicted to be so low that experiments should already have seen some evidence of SUSY particles.

An independent precision determination of α_s is clearly of great value. The scaling violations evident in deep inelastic data offer such an opportunity. In the NLO global analyses of deep inelastic and related data, $\Lambda_{\rm QCD}$, or equivalently $\alpha_s(M_Z)$, is a parameter determined by the fit. A NLO parton analysis [30], which includes the scale dependence uncertainty, gives

$$\alpha_s(M_Z) = 0.109^{+0.004}_{-0.005} \pm 0.003, \tag{22}$$

where the latter error is associated with the scale dependence. Usually scale $\mu = Q$ is chosen in analyses of deep inelastic data. Interestingly it is found [30] that the scale which gives the optimum fit is quite close to this choice and indeed acceptable values of μ are found to lie in a region $0.3Q < \mu < 3Q$ about $\mu = Q$. A related analysis [31], which directly uses the BCDMS structure function data (together with the earlier SLAC measurements), gives

$$\alpha_s(M_Z) = 0.112 \pm 0.003 \pm 0.004.$$

Results (22) and (23), which partly incorporate the same data, are quite compatible with each other and show that the deep inelastic data give a determination of $\alpha_s(M_Z)$ which is very competitive with the LEP measurement given in (21).

5. Small x behaviour of the parton distributions

Essentially there are no experimental measurements in the $x \lesssim 10^{-2}$ (and $Q^2 \gtrsim 5$ GeV^2) region. Does theory have anything to say? Yes, and more interestingly, it predicts the emergence of two new effects as x diminishes: Lipatov 'singular' behaviour and shadowing.

So far we have assumed

$$xg, xq_{\rm sea} \sim \text{const.} \qquad \text{as} \quad x \to 0, \tag{24}$$

based on Regge behaviour applied to the naive parton model. When evolved to higher Q^2 these distributions rapidly develop a steeper shape. It is sufficient to discuss the behaviour of the gluon distribution, since the sea quarks are driven by the gluon and rapidly acquire its small x behaviour. The small x region is dominated by multiple soft gluon emission (arising from the dz/z bremsstrahlung distribution of (10)) and to predict the behaviour

of the gluon we have to sum the contributions arising from a series of diagrams of the type shown in Fig. 12, and possibly also diagrams with virtual corrections. To perform the sum and find the small x behaviour it is useful to relate the contribution, $T_n(x, k_T^2)$, of the ladder diagram with n rungs to that with $n-1$ rungs. Here x and k_T are the longitudinal and transverse momentum of the probed gluon. In the leading $\ln(1/x)$, $\mathrm{LL}(1/x)$, approximation the recursion relation has the general form

$$T_n(x, k_T^2) = \int_x^1 \frac{dx'}{x'} \int dk_T'^2 K(k_T, k_T') T_{n-1}(x', k_T'^2), \tag{25}$$

where the kernel K, which contains a factor of α_s, describes the emission of real gluons as well as allowing for the possibility of including virtual corrections.

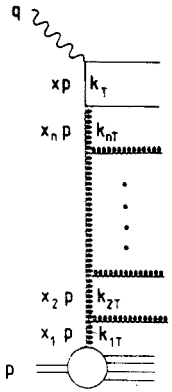

Fig. 12. Diagrammatic representation for probing the gluon content of the proton at small x.

5.1. Double leading logarithm approximation

An estimate of the gluon behaviour at small x and large Q^2 may be obtained using the double leading logarithm approximation, DLLA, in which we keep the leading power of $\ln(1/x)\ \ln Q^2$ at each order in α_s. In axial gauges, the dominant contributions then come from the diagrams like that of Fig. 12 but with both the transverse and longitudinal momenta of the gluons strongly ordered along the chain, that is,

$$Q^2 \gg k_T^2 \gg k_{Tn}^2 \gg \ldots \gg k_{T_1}^2, \qquad x \ll x_n \ldots \ll x_1 \ll 1. \tag{26}$$

In the DLLA the kernel of (25) is particularly simple

$$K(k_T, k'_T) = \frac{3\alpha_s}{\pi k'^2_T}\theta(k^2_T - k'^2_T), \tag{27}$$

where the θ function reflects the ordering in transverse momenta along the chain. If we insert this kernel into (25) we find

$$T_n = \frac{3\alpha_s}{\pi}\frac{\ln(1/x)}{n}\frac{\ln(k^2_T)}{n}T_{n-1}, \tag{28}$$

and on summing over n we obtain

$$\begin{aligned} xg(x,Q^2) &= \sum_n \frac{1}{(n!)^2}\left(\frac{3\alpha_s}{\pi}\ln(1/x)\ln(Q^2)\right)^n \\ &\simeq \exp\left(2\left(\frac{3\alpha_s}{\pi}\ln(1/x)\ln(Q^2)\right)^{\frac{1}{2}}\right), \end{aligned} \tag{29}$$

where we neglect slowly varying functions of the argument of the exponential. Here we have assumed that α_s is constant; if we allow for the running of α_s then $\alpha_s \ln(Q^2)$ becomes proportional to $\ln(\ln(Q^2))$. From (29) we see that $xg(x,Q^2)$ increases, as $x \to 0$, faster than any power of $\ln(1/x)$, but slower than any power of x.

Can we believe the DLLA prediction for the small x behaviour of the gluon? Certainly not at low or medium Q^2. Moreover we have mentioned that the traditional input assumption, $xg \to$ constant as $x \to 0$, is not stable to evolution in Q^2; upwards evolution rapidly generates a sharp peak at very small x and downwards evolution results in a distribution which becomes negative. This assumption is thus suspect.

5.2. Lipatov 'singular' behaviour

To find the form of the small x behaviour of the starting gluon distribution we need to sum the leading $\log(1/x)$ terms, but retain the full Q^2 dependence, not just the leading $\ln(Q^2)$ terms. Clearly we must relax the strong ordering (26) of the k_T's, which generate the $\ln^n(Q^2)/n!$ behaviour, and integrate over the full k_T phase space. The kernel of (25) is then [32,33]

$$K(k_T, k'_T) = \frac{3\alpha_s}{\pi}k^2_T\left(\frac{1}{k'^2_T\,|k^2_T - k'^2_T|} - \beta(k^2_T)\delta(k^2_T - k'^2_T)\right), \tag{30}$$

where

$$\beta(k_T^2) = \int \frac{dk_T'^2}{k_T'^2} \left(\frac{1}{|k_T^2 - k_T'^2|} - \frac{1}{(4k_T'^4 + k_T^4)^{\frac{1}{2}}} \right). \tag{31}$$

The first term in (30) corresponds to diagrams with only real gluon emission, whereas the second allows for diagrams with virtual corrections. The apparent singularity cancels between the real and virtual contributions to the kernel. Insertion of this kernel into (25) gives rise to the so-called Lipatov equation [32,33]. Unlike the DLLA, it is no longer simple to predict the small x behaviour of the gluon. The result turns out to be

$$xg \sim x^{-\lambda} \tag{32}$$

as $x \to 0$, where λ is the maximum eigenvalue of the kernel, (30).

Insight into the derivation of (32) is obtained from a toy model [3] in which it is assumed that the kernel has a factorized form

$$K(k_T, k_T') = u(k_T)v(k_T') \tag{33}$$

although of course, we see the Lipatov kernel (30) has a more complicated structure. Substitution into the recursion formula (25) gives

$$T_n(x, k_T^2) = u(k_T) \int_x^1 \frac{dx'}{x'} \int dk_T'^2 v(k_T') T_{n-1}(x', k_T'^2) \tag{34}$$

which itself is of factorizable form

$$T_n(x, k_T^2) = u(k_T)t_n(x). \tag{35}$$

Rewriting the recursion relation (34) in terms of t_n we obtain

$$t_n(x) = \lambda \int_x^1 \frac{dx'}{x'} t_{n-1}(x'), \tag{36}$$

where

$$\lambda = \int_0^\infty dk_T^2 u(k_T)v(k_T). \tag{37}$$

The nested integrations of (36) give

$$t_n(x) \sim \frac{\lambda^n}{n!} \ln^n(1/x). \tag{38}$$

Summing the t_n over n we thus generate the small x behaviour

$$xg(x,Q^2) \sim h(Q^2)\exp\left(\lambda \ln(1/x)\right) = h(Q^2)x^{-\lambda}, \tag{39}$$

where the exponent λ, defined by (37), can be seen to be the eigenvalue of the kernel, *viz.*,

$$K \otimes u = \int u(k_T)v(k_T')u(k_T')dk_T'^2 = \lambda u. \tag{40}$$

For the actual Lipatov kernel, (30), it can be shown [34], for a running α_s, that the leading eigenvalue λ lies in the range

$$\frac{3.6}{\pi}\alpha_s(k_0^2) \leq \lambda \leq \frac{12\ell n2}{\pi}\alpha_s(k_0^2), \tag{41}$$

where k_0^2 is the infrared cutoff applied to the integrals over the transverse momenta. Taking $\alpha_s \sim 0.25$ we have $\lambda \sim 0.5$, so

$$xg(x,Q^2) \sim h(Q^2)x^{-\frac{1}{2}}. \tag{42}$$

This "singular" behaviour differs appreciably from the traditional "constant" behaviour assumed in (24), and moreover we shall see that it manifests a stability to evolution in Q^2 that was lacking in (24). Table I shows which analyses have allowed for a $\lambda \neq 0$ type of behaviour. However before we consider the phenomenological implications of this behaviour we first discuss the second "new" effect which emerges at very small x, namely "shadowing".

5.3 Shadowing contributions

The increase in $xg(x,Q^2)$, as x decreases, given by (42) (or even (29)), cannot go on indefinitely. If the density of gluons within the proton becomes too large they can no longer be treated as free partons. The growth, as $x \to 0$, must eventually be suppressed by gluon recombination [33,35]. The sketches of Fig. 13 show the gluons found in the proton, first by probing at medium x and secondly at very small x when gluon recombination can no longer be neglected. As x decreases, when do we expect the "shadowing" contributions to start to become appreciable? A back-of-the-envelope estimate can be obtained by viewing the proton from a frame in which its momentum p is large, but in which $xp \gg Q$. A measurement of $g(x,Q^2)$ probes a gluon of transverse size $\sim 1/Q$, but much smaller longitudinal size $\sim 1/px$, so that the proton appears as a thin disc. The number of gluons, n_g, per unit of rapidity is $xg(x,Q^2)$ and the gluon-gluon cross-section $\hat{\sigma} \sim \alpha_s(Q^2)/Q^2$, so the crucial parameter is

$$W \equiv \frac{n_g \hat{\sigma}}{\pi R^2} \sim \frac{\alpha_s(Q^2)}{\pi R^2 Q^2} x g(x, Q^2), \tag{43}$$

where R is the radius of the proton. In regions of x and Q^2 where $W \ll 1$ the interaction of gluons should therefore be negligible and we may continue to evolve in Q^2 as in (9). However, at sufficiently small x, when $W \sim \alpha_s$, the QCD evolution equation must include an additional term [33,35], quadratic in xg,

$$Q^2 \frac{\partial(xg(x,Q^2))}{\partial Q^2} = P_{gg} \otimes g + P_{gq} \otimes q - \frac{81\alpha_s^2(Q^2)}{16R^2Q^2}\theta(x_0 - x)\int_x^{x_0} \frac{dx'}{x'}\Big(x'g(x',Q^2)\Big)^2. \tag{44}$$

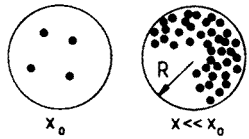

Fig. 13. The gluon content of the proton in the transverse plane

This is frequently called the GLR equation. For convenience this "shadowing" term has only been introduced into the evolution equation for small x, that is $x \leq x_0 = 10^{-2}$ say. The effect of the negative contribution of the shadowing term is to tame the indefinite increase of the gluon distribution leading instead to gluon saturation for sufficiently small values of x and/or Q^2

$$xg^{\text{sat}}(x,Q^2) \propto \frac{Q^2R^2}{\alpha_s(Q^2)}. \tag{45}$$

Before this limit is reached one should take into account higher order shadowing contributions in the evolution equations, which themselves will eventually cease to be valid as we enter the non-perturbative domain with decreasing x.

5.4. Phenomenological Analysis

The last analysis listed in Table I, KMRS [3], incorporates both the singular $x^{-1/2}$ type behaviour and also its suppression by shadowing effects. Predictions obtained from the resulting partons, which are relevant

for HERA, are shown in Fig. 14. It shows F_2^{ep} and the longitudinal structure function, F_L^{ep}, which reflect the small x behaviour of the sea and gluon distributions respectively. In each case 4 predictions are shown, corresponding to the 4 sets of partons obtained by KMRS [3]. The top curve is predicted from set B_- in which the $x^{-1/2}$ behaviour is incorporated but shadowing is omitted. The effect of the inclusion of the shadowing term in (44) is shown for two choices of R, the radius parameter which describes how the gluons are concentrated within the proton. The conventional choice $R = 5$ GeV^{-1} assumes that they are uniformly spread across the proton, whereas the extreme choice $R = 2$ GeV^{-1} assumes that they are concentrated in small "hot-spots" [35,36] within the proton. For comparison Fig. 14 also shows the predictions of a traditional set of partons, B_0, for which λ is taken to be 0 in (13) and (14). We see that the Lipatov $x^{-1/2}$ behaviour really only emerges below $x \simeq$ few $\times 10^{-3}$ and that (conventional) shadowing only gives a noticeable suppression below $x \simeq$ few $\times 10^{-4}$. The available data are equally well fitted by all 4 sets of partons. For example the continuous and dashed curves in Figs 6 and 10 show the descriptions, obtained by the B_- and B_0 sets of partons respectively, to some of the data used in the analysis. Where the dashed curve is not shown it is indistinguishable from the continuous curve. In summary the present data do not confirm one way or the other whether the gluon has the singular $x^{-1/2}$ behaviour, but this is not surprising as it is only expected to become manifest in the region where, as yet, no measurements have been made.

As far as future experiments are concerned we note that the Q^2 evolution, at small x, will be probed over a rather limited range of $\ln Q^2$. This will be particularly true at HERA where information at very small $x(10^{-4} \lesssim x \lesssim 10^{-3})$ is only accessible for relatively low Q^2, typically $Q^2 \sim 10$ GeV^2. Thus the interest focusses on the extrapolation of the input distribution $g(x, Q_0^2)$ into the small x region. In other words it is crucial in the KMRS [3] (or any similar analysis) to choose the appropriate functional behaviour for $g(x, Q_0^2)$ at small x. As mentioned above the KMRS analysis includes both the Lipatov and shadowing effects; a factor $x^{-1/2}$ is inserted in the "starting" gluon and sea distributions (*cf.* (14) and (13)) and then shadowing is incorporated by modifying the distributions at small x so that they approximate a semiclassical solution to the Lipatov equation with quadratic shadowing terms included. Although this procedure is an improvement on previous phenomenological analyses there is clearly quite a bit of ambiguity in the very small x region. It is true that the $x^{-\lambda}$ behaviour is stable to changes of Q^2, but we still have the uncertainty in the choice of the value of λ, which is proportional to $\alpha_s(k_0^2)$, see (41). Also we may question the reliability of the input shadowing form. KMRS used a form which Collins and Kwieciński [37] had obtained by numerically solving the

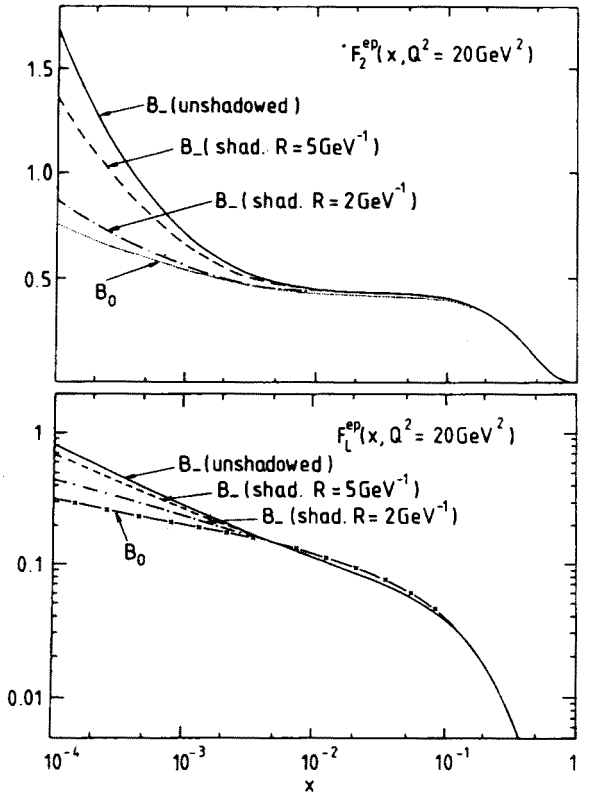

Fig. 14. Predictions for the structure functions F_2 and F_L for deep inelastic ep $\rightarrow$ eX scattering at $Q^2 = 20$ GeV^2 using the 4 different sets of KMRS partons [3].

semiclassical approximation to the DLLA of the Lipatov equation with the shadowing term included. To be precise they used the differential form of (44),

$$\frac{\partial^2(xg(x,Q^2))}{\partial \ln(1/x)\partial \ln(Q^2)} = \frac{3\alpha_s(Q^2)}{\pi} xg(x,Q^2)\left(1 - \frac{27\pi\alpha_s(Q^2)}{16R^2Q^2} xg(x,Q^2)\right), \quad (46)$$

and retained only the first-order derivatives of $\ln(xg(x,Q^2))$. The semiclassical approximation has the advantage that the boundary conditions can be imposed at fixed x_0, in a region where shadowing is negligible, and the equation, with the shadowing term included, can then be solved numerically for $x < x_0$ (using the method of characteristics). The disadvantage is that $g(x_0,Q^2)$ has to be supplied over a range of Q^2 right down to the non-perturbative region $Q^2 \gtrsim \Lambda^2$. Clearly it is important to investigate the validity of this approach.

5.5. *Numerical solution of the Lipatov and GLR equations*

The Lipatov equation with shadowing contributions included is frequently called the GLR [33] equation. It is clearly desirable to directly solve the GLR equation to see if the $x^{-\lambda}$-type behaviour emerges and to quantify the suppression due to shadowing. Now the GLR equation may be written in the differential form (*cf.* the DLLA of (46))

$$x\frac{\partial f(x,k_T^2)}{\partial x} = \int_{k_0^2}^{\infty} dk_T'^2 K(k_T,k_T')f(x,k_T'^2) - \frac{81\alpha_s^2(k_T^2)}{16R^2k_T^2}\left(xg(x,k_T^2)\right)^2, \quad (47)$$

where K is the Lipatov kernel, (30), and f is the gluon distribution before the integration over the transverse momentum has been performed

$$f(x,k_T^2) = \frac{\partial(xg(x,k_T^2))}{\partial \ln k_T^2}. \quad (48)$$

While the linear term on the right hand side of (47) generates contributions which go beyond the LL(Q^2) approximation, the quadratic shadowing term is still within this approximation. Also only the leading order shadowing contribution is included. As we proceed to ultra-small x, first higher order shadowing corrections and then non-perturbative effects will become important. The GLR equation, (47), is based on the perturbative form of the gluon propagator and so, as it stands, it is not valid at low values of k_T^2 and $k_T'^2$; an explicit lower limit k_0^2 is therefore imposed on the transverse momenta of the exchanged gluons, *i.e.*, $k_T^2, k_T'^2 > k_0^2$. Moreover since (47) arises from LL($1/x$) approximation it is only valid in the small x region.

Recently the non-linear integro-differential GLR equation, (47), for the gluon distribution has been solved [38] in the $x < x_0 \equiv 10^{-2}$ region, taking the boundary conditions, $g(x_0,Q^2)$, from KMRS [3]. The gluon distributions so obtained are compared in Fig. 15 with the KMRS gluons extrapolated to small x at four different values of Q^2; in each case the three curves correspond, in descending order, to the gluon with shadowing neglected and with shadowing included with R = 5 and 2 GeV^{-1}.

Several features of Fig. 15 are worth mentioning. First we notice that the explicit unshadowed solution (the upper continuous curve) exhibits the advertised $x^{-\lambda}$ behaviour with a value of λ, $\lambda = 0.47$, which is similar to that used in the phenomenological analyses [3,19] and which is remarkably stable to evolution in Q^2. On the other hand λ depends on the infrared cutoff, k_0^2, on the integration over the gluon transverse momentum; for example, we find $\lambda = 0.47$ or 0.42 or 0.37 depending on whether the cutoff

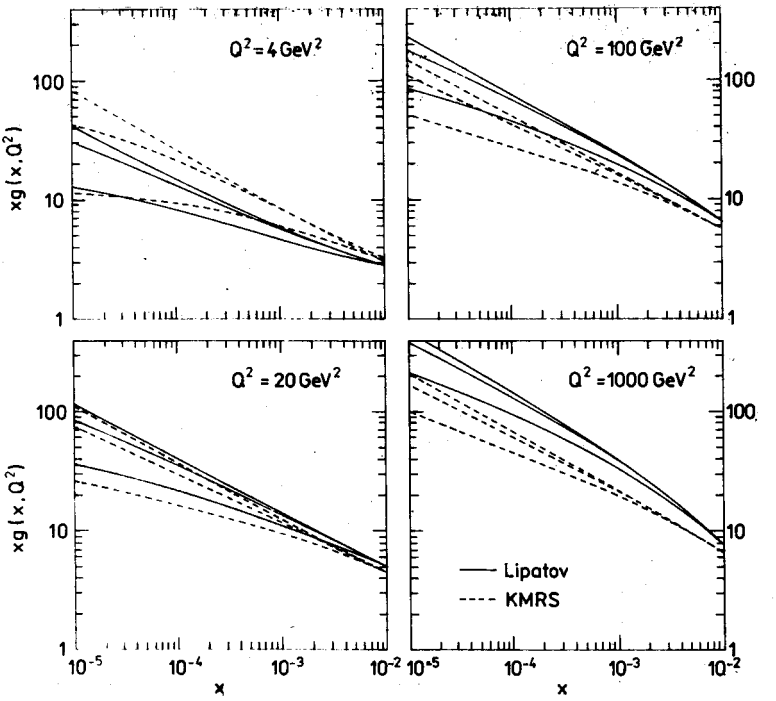

Fig. 15. The continuous curves, in descending order, are the values of $xg(x,Q^2)$ determined by solving the Lipatov equation without and with the shadowing term included (with $R = 5$ and 2 GeV^{-1} respectively). The dashed curves correspond to the gluons from KMRS [3] (set B_-, without and with shadowing). The different curvatures of the continuous and dashed curves near $x = x_0 = 10^{-2}$ are an artefact of using (KMRS) boundary conditions which evolve in Q^2 slower than the solution of the equation. The figure is taken from Ref. [38].

is chosen to be 1 or 2 or 4 GeV^2. Secondly we see from Fig. 15 that the explicit solutions (the continuous curves) have similar x dependence and shadowing contributions to that found by KMRS [3] (the dashed curves), but that they evolve faster in Q^2 than the KMRS gluons. Indeed it is found that the Lipatov equation generates gluons which evolve in Q^2 at essentially the same rate as the double leading logarithm (DLLA) evolution [39,38]. The differing rates of evolution seen in Fig. 15 can therefore be traced to the difference between DLLA evolution and the complete Altarelli–Parisi leading (and next-to-leading) $\ln Q^2$ evolution used by KMRS. Keeping just the leading behaviour of the gluon splitting function, $P_{gg}(z) \sim 6/z$, as in DLLA, is known to lead to a too rapid an evolution in Q^2. This suggests that the Lipatov equation should be extended to incorporate terms that are non-leading in $\ln(1/x)$ but yet which are important for the Q^2 evolution.

Until this is done we conclude that the most reliable procedure is to use the GLR equation to generate the shape of the very small x behaviour of the gluon and then to evolve in Q^2 using the complete Altarelli–Parisi equations.

Finally we note the explicit solutions of the GLR equation have been used [38] to delineate the (x, Q^2) domain of validity of the leading order shadowing approximation.

5.6. Experimental probes of very small x

HERA will soon probe F_2^{ep} (and eventually F_L^{ep}) down to $x \sim 10^{-3}$ and as the luminosity increases it may be possible to extend the measurements to $x \sim 10^{-4}$ at $Q^2 = 10$ GeV^2. This should reveal the behaviour of the sea (and the gluon [40]) distribution at small x. Also the measurement of inelastic J/ψ production at HERA can probe the gluon at small x [41].

As we have mentioned before, the existing experimental data (which do not extend into the region $x < 10^{-2}$) do not show any evidence of a Lipatov $x^{-\lambda}$-type growth of the gluon (and sea) as x decreases. We see from Fig. 14 that the identification of this behaviour, even from measurements at HERA, will not be easy. It is therefore desirable to look for processes specifically designed to expose the Lipatov behaviour. One such novel method has been proposed by Mueller [6] ; that is to see if there is a possible $x^{-\lambda}$ type growth, with decreasing x, of the cross section for a deep inelastic event containing an associated jet as a function of x_1/x, where x_1 is the longitudinal momentum fraction carried by the measured jet (x_1 is kept fixed).

Finally we note that the LHC and SSC offer the opportunity of determining the sea quark distribution at surprising small x by studying Z production at large rapidity [42,3]. At large rapidity a sizeable contribution to the cross section arises from $q_v \bar{q}_s$ annihilation and since the valence distribution peaks at $x_{val} \sim 0.1$ it means we are probing the sea at $x_{sea} \sim M_Z^2/s x_{val} \sim 10^{-4}$. Even smaller x could be probed if Drell–Yan pairs [43,42] could be isolated from the leptons arising from heavy quark decays.

6. Conclusions

There has been a considerable improvement in the precision of the deep inelastic scattering data and also of the data for prompt photon production and the Drell–Yan process. This, combined with the knowledge of the next-to-leading order QCD contributions, has enabled well-constrained sets of parton distributions of the proton to be determined, at least in the region $0.03 \lesssim x \lesssim 0.8$ where the data exist. These data also allow $\alpha_s(M_Z)$ to be determined; the two recent analyses [30,31] of deep inelastic data give an average value

$$\alpha_s(M_Z) = 0.110 \pm 0.007,$$

with an accuracy comparable to the independent determination from the LEP experiments.

The situation is much less clear in the small x region, that is $x \lesssim 10^{-2}$. We discussed two new theoretical effects which are expected to occur at small x. First by summing the leading $\ln(1/x)$ terms, according to the Lipatov equation [32], it is predicted that the gluon and sea distributions (or, to be precise, xg and $xq_{\rm sea}$) will show a 'singular' $x^{-\lambda}$ behaviour, as $x \to 0$, with $\lambda \sim 0.5$. The present data do not determine, or indeed show any evidence of, this singular behaviour, but this is not surprising as it is only expected to become manifest below $x \sim 10^{-3}$. The second effect is shadowing; the $x^{-\lambda}$ growth cannot continue indefinitely but will be suppressed by gluon recombination or shadowing contributions.

We showed results from a recent parton analysis of deep inelastic and related data (KMRS [3]) which incorporated both the $x^{-1/2}$ behaviour and its suppression by shadowing. If we assume that the gluons are spread uniformly across the proton, and that they are not concentrated in hot-spots, it is found that the shadowing corrections are small; even at $x \sim 10^{-4}$ they lead to only about a 20% suppression in the predicted values of $F_2^{\rm ep}$ and $F_{\rm L}^{\rm ep}$ (see Fig. 14).

We also briefly discussed an explicit solution of the Lipatov equation with shadowing (or, as it is known, the GLR [33] equation). In this way we were able to explicitly see the emergence of the $xg \sim x^{-\lambda}$ behaviour, and found, as anticipated, that it was stable to evolution in Q^2 (see Fig. 15). The actual value of λ was dependent on the infrared cutoff; for example, it is found that the numerical solution has $\lambda = 0.47$ or 0.42 according to whether the cutoff is chosen to be 1 or 2 GeV^2. The effect of the shadowing correction on the numerical solution was seen to be similar to that in the phenomenological KMRS analysis. However the Q^2 evolution of the gluon was faster than theoretical expectations and indicated that leading $\ln Q^2$ terms, which are non-leading in $\ln(1/x)$, should be included in the GLR framework.

In conclusion it is clear that much theoretical work has yet to be done to obtain unambiguous perturbative QCD predictions at small x, and it is hoped that the interplay between theory and the results of the forthcoming experiments (at HERA and elsewhere) will illuminate this interesting problem.

I thank Peter Harriman, Jan Kwieciński, Dick Roberts, James Stirling and Peter Sutton for very enjoyable research collaborations during our studies of parton distributions.

I also thank all the organizers for their extremely warm hospitality during the Cracow School of Theoretical Physics in Zakopane.

REFERENCES

[1] R.E. Taylor, H.W. Kendall, J.I. Friedman, *Rev. Mod. Phys.* **63**, 573, 597, 615 (1991).
[2] BCDMS collaboration: A.C. Benvenuti *et al.*, *Phys. Lett.* **223B**, 485 (1989).; *Phys. Lett.* **237B**, 599 (1990).
[3] J. Kwieciński, A.D. Martin, R.G. Roberts, W.J. Stirling, *Phys. Rev.* **D42**, 3645 (1990).
[4] Recent reviews of parton distributions include R.G. Roberts, *The Structure of the Proton*, Cambridge Univ. Press, 1991. R.K. Ellis, W.J. Stirling, CERN Yellow report 91-01, 1991 p.135; Proc. of the Workshop on Hadronic structure functions and parton distributions, FNAL April 1990, eds D.F. Geesaman, J. Morfin, C. Sazama, W.-K. Tung, World Scientific, 1990; J. Bartels, *Particle World* **2**, 46 (1991); E. Reya, Proc. of the Workshop on High energy physics phenomenology II, Calcutta, Jan. World Scientific 1991; B. Badelek, K. Charchula, M. Krawczyk, J. Kwieciński, to be published.
[5] S.D. Ellis, Z. Kunszt, D.E. Soper, *Phys. Rev. Lett.* **64**, 2121 (1990) and private communication.
[6] A.H. Mueller, *Nucl. Phys. B* (Proc. Suppl.). **18C**, 125 (1990).
[7] CDHSW Collaboration: H. Abramowitcz *et al.*, *Z. Phys.* **C15**, 19 (1982); CCFRR Collaboration: C. Foudas *et al.*, *Phys. Rev. Lett.* **64**, 1207 (1990).
[8] NM Collaboration: D. Allasia *et al.*, *Phys. Lett.* **294B**, 366 (1990); *Phys. Rev. Lett.* **66**, 2712 (1991).
[9] M. Glück, E. Hoffman, E. Reya, *Z. Phys.* **C13**, 119 (1982).
[10] D.W. Duke, J.F. Owens, *Phys. Rev.* **D30**, 49 (1984).
[11] E. Eichten, I. Hinchliffe, K. Lane, C. Quigg, *Rev. Mod. Phys.* **56**, 579 (1984).; erratum **58**, 1065 (1986).
[12] EM Collaboration: J.J. Aubert *et al.*, *Nucl. Phys.* **B259**, 189 (1985); **B293**, 740 (1987).
[13] CDHSW Collaboration: J.P. Berge *et al.*, CERN preprint EP89-103 (1989).
[14] CCFRR Collaboration: E. Oltman, Columbia University thesis, Nevis Report No. 270.
[15] A.D. Martin, R.G. Roberts, W.J. Stirling, *Phys. Rev.* **D37**, 1161 (1988); see also *Phys. Lett.* **206B**, 327 (1988); *Mod. Phys. Lett.* **A4**, 1135 (1989).
[16] M. Diemoz, F. Ferroni, E. Longo, G. Martinelli, *Z. Phys.* **C39**, 21 (1988).
[17] P. Aurenche, R. Baier, M. Fontannaz, J.F. Owens, M. Werlen, *Phys. Rev.* **D39**, 3275 (1989).
[18] P. Harriman, A.D. Martin, R.G. Roberts, W.J. Stirling, *Phys. Rev.* **D42**, 798 (1990).
[19] J.G. Morfin, W.-K. Tung, Fermilab preprint 90/74 (1990).
[20] M. Glück, E. Reya, A. Vogt, *Z. Phys.* **C48**, 471 (1990).

[21] A.D. Martin, R.G. Roberts, W.J. Stirling, *Phys. Rev.* **D43**, 3648 (1991).
[22] WA70 Collaboration: M. Bonesini *et al.*, *Z. Phys.* **C38**, 371 (1988).
[23] CHARM: F. Bergsma *et al.*, *Phys. Lett.* **123B**, 269 (1983).
[24] E288 Collaboration: A.S. Ito *et al.*, *Phys. Rev.* **D23**, 604 (1981); E605 Collaboration: C.N. Brown *et al.*, *Phys. Rev. Lett.* **63**, 2637 (1989).
[25] L.W. Whitlow *et al.*, in Proc. of the Workshop on Hadron Structure Functions and Parton Distributions, FNAL, April 1990, eds D.F. Geesaman *et al.*, World Scientific p. 67.
[26] M. Virchaux, in Proc. of the Workshop on Hadron Structure Functions and Parton Distributions, FNAL, April 1990, eds D.F. Geesaman *et al.*, World Scientific, p. 124.
[27] W.J. Stirling, A.D. Martin, *Phys. Lett.* **B237**, 551 (1990).
[28] U. Amaldi, W. de Boer, H. Furstenau, *Phys. Lett.* **B260**, 447 (1991).
[29] T. Hebbeker, Proc. of Int. Lepton-Photon Symposium on HE Physics, Geneva, July 1991.
[30] A.D. Martin, W.J. Stirling, R.G. Roberts, *Phys. Lett.* **B266**, 173 (1991).
[31] M. Virchaux, Proceedings of the XI Int. Conf. on "Physics in Collision" Colmar, June 1991.
[32] E.A. Kuraev, L.N. Lipatov, V.S. Fadin, *Sov. Phys. JETP* **44**, 443 (1976); **45**, 199 (1977); Ya.Ya. Balitsky, L.N. Lipatov, *Sov. J. Nucl. Phys.* **28**, 822 (1978); L.N. Lipatov, *Phys. Lett.* **251B**, 284 (1990); L.N. Lipatov, R. Kirschner, *Z. Phys.* **C45**, 477 (1990); M. Ciafaloni, *Nucl. Phys.* **B296**, 49 (1988).
[33] L.V. Gribov, E.M. Levin, M.G. Ryskin, *Phys. Rep.* **100**, 1 (1983).
[34] J.C. Collins, J. Kwieciński, *Nucl. Phys.* **B316**, 307 (1989).
[35] A.H. Mueller, J. Qiu, *Nucl. Phys.* **B268**, 427 (1986).
[36] E.M. Levin, M.G. Ryskin, *Phys. Rep.* **189**, 267 (1990).
[37] J.C. Collins, J. Kwiecinski, *Nucl. Phys.* **B335**, 89 (1990).
[38] J. Kwieciński, A.D. Martin, P.J. Sutton, *Phys. Lett.* **264B**, 199 (1991); *Phys. Rev.* **D44**, (in press).
[39] E.M. Levin, G. Marchesini, M.G. Ryskin, B.R. Webber, *Nucl. Phys.* **B357**, 167 (1991).
[40] A.M. Cooper-Sarkar *et al.*, *Z. Phys.* **C39**, 281 (1988).
[41] A.D. Martin, C.-K. Ng, W.J. Stirling, *Phys. Lett.* **B191**, 200 (1987); S.M. Tkaczyk, W.J. Stirling, D.H. Saxon, Proc. HERA Workshop, DESY 1988, Vol. 1, p. 265; Z. Kunszt, *Phys. Lett.* **B207**, 103 (1988); K.J. Abraham, *Phys. Lett.* **B240**, 224 (1990); NIKHEF preprint H-91-02 (1991); M. Drees, C.S. Kim, DESY preprint 91-085 (1991).
[42] A.D. Martin, W.J. Stirling, *Phys. Lett.* **B248**, 443 (1990).
[43] J.G. Morfin, W.-K. Tung, Fermilab preprint-90/24 (1990); F. Olness, W.-K. Tung, *J. Mod. Phys.* **A2**, 1413 (1987).